PERGAMON International Journal of Multiphase Flow 24 (1998) 1005–1023

International Journal of Multiphase Flow

Mathematical model and numerical simulation of the settling of flocculated suspensions

R. Bürger [a,*], F. Concha [b]

[a] *Mathematisches Institut A, University of Stuttgart, Pfaffenwaldring 57, D-70569, Stuttgart, Germany*
[b] *Department of Metallurgical Engineering, University of Concepción, Casilla 53-C, Correo 3, Concepción, Chile*

Received 18 May 1997; received in revised form 1 May 1998

Abstract

Thickeners for solid–liquid separation are still designed and controlled empirically in the mining industry. Great efforts are being made to develop mathematical models that will change this situation. Starting from the basic principles of continuum mechanics, the authors developed a phenomenological theory of sedimentation for flocculated suspensions which takes the compressibility of the flocs under their own weight and the permeability of the sediment into consideration. This model yields, for one space dimension, a first-order hyperbolic partial differential equation for the settling and a second-order parabolic partial differential equation for the consolidation of the sediment, where the location of the interface with the change from one equation to the other is, in general, unknown beforehand. This initial-boundary value problem was analyzed mathematically, and transient solutions are obtained for several continuous feed and discharge flows. A finite difference numerical method is used to calculate concentration profiles of the transient settling process, including the filling up and emptying of a thickener.

Keywords: Sedimentation; Continuous thickening; Degenerate parabolic quasilinear partial differential equation; Flocculated suspension

1. Introduction

The settling of flocculated suspensions is a subject that has attracted the attention of many authors. From the early works of Mishler (1912) and Coe and Clevenger (1916) to the recent book edited by Tory (1996), several research workers and engineers have contributed to a theory of thickening. Many of these works have been of empirical nature, but in the last

* Corresponding author. Fax: 0049-711-6855599; E-mail: buerger@mathematik. uni-stuttgart.de.

0301-9322/98/$19.00
PII: S0301-9322(98)00026-3

twenty years, a phenomenological theory has evolved that permits a clear understanding of the phenomena occurring during the sedimentation in settling columns and in continuous thickeners. The book by Tory (1996) gives a thorough review of this theory.

In spite of the fact that the phenomenological theory of sedimentation is widely accepted, only steady state solutions have been discussed and used for thickener design, as reviewed by Concha and Barrientos (1993). In this work, we present a transient solution to batch and continuous sedimentation of flocculated suspensions.

The phenomenological model leads to a scalar conservation law valid in the interior of the thickener which is of the hyperbolic type [corresponding to the theory of Kynch (1952)] for hindered settling and of the parabolic type for the compressible sediment layer. The location of the interface between both is, in general, unknown beforehand, which constitutes the main mathematical difficulty of the model. Initial and boundary conditions to describe the initial concentration and the feeding and discharge conditions complete the sedimentation process.

In Section 1, we briefly summarize the model describing the settling behaviour of a flocculated suspension in a continuous thickener, which results in the initial-boundary value problem mentioned above. This problem was analyzed by Bürger (1996) and by Bürger and Wendland (1998a, b). The results will be addressed in Section 2. In Section 3 we suggest a numerical algorithm to solve the problem and present numerical examples for several transient batch and continuous sedimentation processes. In Section 4, we discuss our results.

2. Phenomenological theory of sedimentation with compression

2.1. The ideal continuous thickener

We consider sedimentation in a so-called ideal continuous thickener (ICT) as shown in Fig. 1. An ICT is a cylindrical vessel showing no wall effects and in which all field variables are assumed to be constant across each cross section so that they depend only on the variables height z and time t. At height $z = L$, a surface feed and at $z = 0$, a surface discharge are provided for continuous operation. An ICT without feed or discharge is a settling column for batch sedimentation, which we will include as a special case. Furthermore, we assume that the flocs begin to touch each other at a critical volumetric solid concentration value ϕ_c, while they perform hindered settling for volumetric solid concentrations $\phi < \phi_c$.

2.2. Constitutive assumptions

The description of the flocculated suspension (see Concha et al., 1996) requires several constitutive assumptions to specify the choice of material, flocculant, thickener design and manner of operation:

1. the solid particles are small with respect to the sedimentation vessel and have the same density;
2. the solid and liquid components of the suspension are incompressible and there is no mass transfer between them;

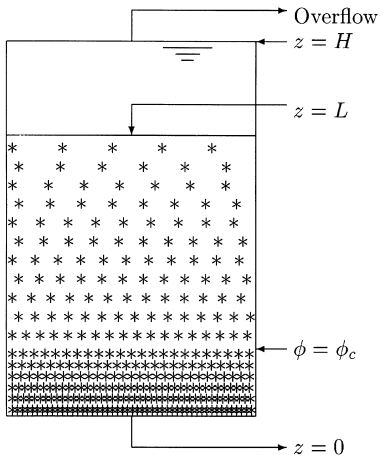

Fig. 1. Ideal continuous thickener (ICT).

3. the suspension is entirely flocculated at the beginning of the sedimentation process;
4. the solid component can perform only a one-dimensional simple compression motion;
5. both solid and liquid components behave as elastic, that is, inviscid fluids;
6. gravitation is the only body force.

Such a suspension can be considered as superimposed continuous media with two components. We note that the assumption that the fluid behaves as an inviscid fluid is based on the assumption that the friction associated with the fluid–fluid interaction, that is, the viscous fluid stress, is much smaller than the one associated with the solid–fluid interaction (Whitaker, 1986; Concha et al., 1996). Therefore, the viscous fluid stress will be neglected. The solid component will be regarded as an elastic fluid as well, since a specific solid concentration is associated with each weight of solid in the sediment. These two assumptions are also made in the rheological model of flocculated suspensions by Landman and White (1994).

2.3. Dynamic sedimentation process

These assumptions lead to four scalar field equations valid wherever the variables are smooth,

$$\frac{\partial \phi}{\partial t} + \frac{\partial}{\partial z}(\phi v_s) = 0, \tag{1}$$

$$\frac{\partial \hat{q}}{\partial z} = 0, \tag{2}$$

$$\rho_s \left[\frac{\partial}{\partial t}(\phi v_s) + \frac{\partial}{\partial z}(\phi v_s^2) \right] = -\frac{\partial p_s}{\partial z} - \rho_s \phi g + \beta(\phi)\frac{\partial \phi}{\partial z} - \alpha(\phi) v_r, \tag{3}$$

$$\rho_f\left\{\frac{\partial}{\partial t}[(1-\phi)v_f]+\frac{\partial}{\partial z}[(1-\phi)v_f^2]\right\}=-\frac{\partial p_f}{\partial z}-\rho_f(1-\phi)g-\beta(\phi)\frac{\partial\phi}{\partial z}+\alpha(\phi)v_r. \tag{4}$$

Here, v_s and v_f are the solid and fluid component velocities, $\hat{q}=\phi v_s+(1-\phi)v_f$ is the volume average velocity of the suspension which can be controlled externally, $v_r=v_s-v_f$ is the relative solid–fluid velocity, ρ_s and ρ_f are the solid and fluid mass densities, p_s and p_f are the solid and fluid pressures, g is the acceleration of gravity, and $\alpha(\phi)$ and $\beta(\phi)$ are scalar functions defining the solid-fluid interaction force per unit volume. Together with the appropriate Rankine–Hunoniot jump conditions (Concha et al., 1996), these equations form a dynamical sedimentation process.

2.4. Simplifcations

First, we introduce characteristic variables, namely, the height of the thickener assumed to be $H\approx 1$ m, the falling velocity of a single solid particle, $v_\infty\approx 10^{-4}$ m s^{-1}, and the time a single floc needs to fall through the thickener, $t_0=H/v_\infty\approx 10^4$ s. Rewriting Eqs. (1) to (4) with dimensionless variables using these quantities, the left-hand sides of the linear momentum equations will contain the Froude number of the flow, $\mathrm{Fr}=v_\infty^2/(Hg)$ as a factor, and will be neglected as $\mathrm{Fr}\approx 10^{-9}$. Next, the theoretical variables p_f and p_s are replaced by experimental variables, viz. the pore pressure p and the effective solid stress σ_e, where

$$p_t(z,t)=p_f(z,t)+p_s(z,t)=p(z,t)+\sigma_e(z,t) \tag{5}$$

is valid for the total pressure p_t. Assuming that the volume porosity in the sediment equals the surface porosity, we obtain $p_f=(1-\phi)p$ and $p_s=\phi p+\sigma_e$, and from (3) and (4)

$$\frac{\partial}{\partial z}(\phi p)+\frac{\partial}{\partial z}\sigma_e=-\rho_s\phi g+\beta(\phi)\frac{\partial\phi}{\partial z}-\alpha(\phi)v_r, \tag{6}$$

$$\frac{\partial}{\partial z}[(1-\phi)p]=-\rho_f(1-\phi)g-\beta(\phi)\frac{\partial\phi}{\partial z}+\alpha(\phi)v_r. \tag{7}$$

Considering (7) at equilibrium, which is attained for $t\to\infty$ in a settling column, the general expression $\beta(\phi)=p(\phi)$ is obtained. Inserting this and the excess pore pressure $p_e=p-\rho_f g(H-z)$ (which is an experimental variable as well) into (6) and (7) simplifies these equations to

$$\frac{\partial\sigma_e}{\partial z}=-\Delta\rho\phi g-\frac{\alpha(\phi)v_r}{1-\phi},\quad \Delta\rho=\rho_s-\rho_f, \tag{8}$$

$$\frac{\partial p_e}{\partial z}=\frac{\alpha(\phi)v_r}{1-\phi}. \tag{9}$$

Consequently, the material specific behaviour of the suspension is described only by the choice of the functions $\alpha(\phi)$ and $\sigma_e(\phi)$ in Eq. (8). For the solid volume flux per unit area given by ϕv_s, we obtain from (8) and the definition of $\hat{q}$

$$\phi v_s = \hat{q}\phi - \frac{\phi(1-\phi)^2}{\alpha(\phi)}\left[\Delta\rho\phi g + \frac{\partial\sigma_e(\phi)}{\partial z}\right]. \tag{10}$$

Obviously, $\sigma_e(\phi) = 0$ for $\phi < \phi_c$ is valid, and σ_e is a monotonically increasing function of ϕ for $\phi \geqslant \phi_c$. Thus, the choice of σ_e satisfying this and

$$\sigma_e'(\phi)\begin{cases} = 0 & \text{for} \quad \phi < \phi_c, \\ \geq 0 & \text{for} \quad \phi \geq \phi_c \end{cases}$$

is made with parameters to be obtained from experiments. We introduce the batch Kynch solid flux density function $\hat{f}_{bk}$ and the solid flux density function $\hat{f}$:

$$\hat{f}_{bk}[\phi(z,t)] = -\Delta\rho g\frac{\phi^2(1-\phi)^2}{\alpha(\phi)}, \quad \hat{f}[\phi(z,t),t] = \hat{q}(t)\phi + \hat{f}_{bk}(\phi).$$

Note that the choice of a functional form for $\hat{f}_{bk}$ is equivalent to choosing one for $\alpha(\phi)$. Using the new variables $q(t) = \hat{q}(t)/L$, $f_{bk}(\phi) = \hat{f}_{bk}(\phi)/L$, $f(\phi, t) = \hat{f}(\phi, t)/L$ and $f(\phi) = \hat{f}(\phi)/L$, and considering the dimensionless independent variable $x = z/L$ and the dimensionless field variable $u(x, t) = \phi(Lx, t)$, the continuity Eq. (1) takes the form

$$\frac{\partial}{\partial t}u(x,t) + \frac{\partial}{\partial x}f(u,t) = \frac{\partial}{\partial x}\left(-f_{bk}(u)\frac{\sigma_e'(u)}{L\Delta\rho ug}\frac{\partial u}{\partial x}\right), \tag{11}$$

where $\hat{q} = \hat{q}(t)$ for smooth regions is a result of (2). We note that for $u < \phi_c$ the parabolic Eq. (11) degenerates into the hyperbolic equation

$$\frac{\partial}{\partial t}u(x,t) + \frac{\partial}{\partial x}[q(t)u + f_{bk}(u)] = 0$$

of Kynch's theory for continuous thickening (see Bustos and Concha, 1996; Bustos et al., 1990a). In general, (11) is a quasilinear degenerate parabolic partial differential equation where, by introducing the notation

$$a(u) = -f_{bk}(u)\frac{\sigma_e'(u)}{L\Delta\rho gu} \tag{12}$$

and requiring that $q(t) \leqslant 0$ and

$$f_{bk}(0) = f_{bk}(1) = 0, \quad f_{bk}(u) < 0 \text{ for } 0 < u < 1,$$

the degeneracy

$$a(u)\begin{cases} = 0 \text{ for } u < \phi_c: & \text{(11) is hyperbolic;} \\ > 0 \text{ for } \phi_c \leq u < 1: & \text{(11) is parabolic;} \\ = 0 \text{ for } u \geq 1: & \text{(11) is hyperbolic} \end{cases}$$

becomes evident. Putting formally $f_{bk}(u) = 0$ for $u < 0$ and $u > 1$, we see that (11) degenerates into the scalar convective equation

$$\frac{\partial u}{\partial t} + q(t)\frac{\partial u}{\partial x} = 0$$

for $u < 0$ and $u > 1$. However, these cases have no physical meaning and can be excluded (Bürger and Wendland, 1998a). The location of the type change is not known beforehand. We are interested in solutions of Eq. (11) on a space-time "cylinder" $\bar{Q}_T = \{(x,\ t)\colon\ 0 \leqslant x \leqslant 1,\ 0 \leqslant t \leqslant T\}$, and assume that the following initial and boundary conditions are given: for $t = 0$, an initial concentration profile $u_0(x)$, $0 \leqslant x \leqslant 1$ is given, at $x = 1$, a concentration value $\phi_1(t)$ is prescribed for $0 \leqslant t \leqslant T$, and the control of the discharge at $x = 0$ corresponds to prescribing that the solid volume flux density across $z = 0$ should reduce to $\hat{q}(t)\phi(0,\ t)$, i.e.

$$f_{bk}(u) - a(u)\frac{\partial u}{\partial x}\bigg|_{x=0} = 0, \quad 0 \leq t \leq T$$

should be valid.

For the calculation of the excess pore pressure p_e, we obtain from Eqs. (8) and (9)

$$\frac{\partial p_e}{\partial z} = -\Delta\rho\phi g - \frac{\partial \sigma_e}{\partial z} = -\Delta\rho\phi g\left[1 + \frac{\sigma_e'(\phi)}{\Delta\rho\phi g}\frac{\partial \phi}{\partial z}\right]$$

and thus

$$\frac{\partial p_e}{\partial x} = -L\Delta\rho\phi g\left[1 + \frac{\sigma_e'(u)}{L\Delta\rho u g}\frac{\partial u}{\partial x}\right] = -L\Delta\rho u g\left[1 - \frac{a(u)}{f_{bk}(u)}\frac{\partial u}{\partial x}\right]. \tag{13}$$

Note that the excess pore pressure field can be calculated after $u(x,\ t)$ has been calculated on $\bar{Q}_T$. An appropriate boundary condition for the integration of (13) from $x = 1$ to $x = 0$ is

$$p_e(1) = 0 \tag{14}$$

(Concha et al., 1996), hence we obtain

$$p_e(x,\ t) = L\Delta\rho g\int_x^1 u(\xi,\ t)\left[1 - \frac{a[u(\xi,\ t)]}{f_{bk}[u(\xi,\ t)]}\frac{\partial u}{\partial \xi}(\xi,\ t)\right]\mathrm{d}\xi. \tag{15}$$

However, since it is possible to calculate the pressure *a posteriori*, this quantity will not be included in the formulation of the initial-boundary value problem.

Furthermore, using (10) and the definition of $\hat{q}(t)$, the solid and fluid phase velocities can be written as

$$v_s = \hat{q}(t) + \frac{\hat{f}_{bk}(\phi)}{\phi}\left[1 + \frac{\sigma_e'(\phi)}{\Delta\rho\phi g}\frac{\partial \phi}{\partial z}\right], \quad v_f = \hat{q}(t) - \frac{\hat{f}_{bk}(\phi)}{1-\phi}\left[1 + \frac{\sigma_e'(\phi)}{\Delta\rho\phi g}\frac{\partial \phi}{\partial z}\right]$$

or as

$$v_s = L\left\{q(t) + \frac{f_{bk}(u)}{u}\left[1 + \frac{\sigma_e'(u)}{L\Delta\rho u g}\frac{\partial u}{\partial x}\right]\right\}, \quad v_f = L\left\{q(t) - \frac{f_{bk}(u)}{1-u}\left[1 + \frac{\sigma_e'(u)}{L\Delta\rho u g}\frac{\partial u}{\partial x}\right]\right\}. \tag{16}$$

3. Mathematical model

Summarizing, the following initial-boundary value problem (IBVP) should be considered:

$$\frac{\partial u}{\partial t}+\frac{\partial}{\partial x}f(u,t)=\frac{\partial}{\partial x}\left(a(u)\frac{\partial u}{\partial x}\right),\quad (x,t)\in Q_{\mathrm{T}}=(0,1)\times(0,T), \tag{17}$$

$$\begin{aligned} u(x,0)&=u_0(x),\quad 0\le x\le 1,\\ f_{\mathrm{bk}}(u)-a(u)\frac{\partial u}{\partial x}\bigg|_{x=0}&=0,\quad 0\le t\le T,\\ u(1,t)&=\phi_1(t),\quad 0\le t\le T. \end{aligned} \tag{18}$$

Since Eq. (17) is nonlinear, the solution might develop discontinuities even if the initial and boundary data are smooth, hence we have to consider weak solutions of the IBVP. To obtain uniqueness, a weak solution must satisfy an additional entropy criterion or selection principle. In this case, it will be a generalized solution. Existence and uniqueness of generalized solutions, as well as entropy boundary and jump conditions, were obtained by Bürger (1996) and by Bürger and Wendland (1988a, b). We refer to these works and to the review article by Concha and Bürger (1998) for details.

4. Numerical solution

4.1. Numerical algorithm

The approximate solution to the IBVP is obtained by operator splitting. To calculate an approximation v for the first time step:

1. calculate $\hat{v}(x,\Delta t)$ as the approximate solution of $v_t=(a(v)v_x)_x$ with $v(x,0)=u_0(x)$ and boundary conditions evaluated at $t=\Delta t$;
2. if $q(0)<0$, then calculate $\tilde{v}(x,\Delta t)$ as the solution of the linear convective equation $v_{\mathrm{t}}+q(0)v_x=0$ setting $v(x,0)=\hat{v}(x,0)$, evaluated at $t=\Delta t$, otherwise put $\tilde{v}(x,\Delta t)=\hat{v}(x,\Delta t)$;
3. calculate $v(x,\Delta t)\approx u(x,\Delta t)$ as the solution of the hyperbolic conservation law $v_{\mathrm{t}}+(f_{\mathrm{bk}}(v))_x=0$ with $v(x,0)=\tilde{v}(x,\Delta t)$ and with boundary conditions.

The numerical treatment of these steps is the following:

1. The diffusion term is discretized implicitly (as otherwise the CFL condition would preclude calculations with a fixed value of $\lambda=\Delta t/\Delta x=$ const.) in the form

$$a(u)\frac{\partial u}{\partial x}\approx\theta a_j^{n+1}\left(\frac{\partial u}{\partial x}\right)^{n+1}+(1-\theta)a_j^n\left(\frac{\partial u}{\partial x}\right)^n,\quad \theta\in[0,1]$$

where $\theta=0$ corresponds to a fully explicit, $\theta=1$ to a fully implicit scheme; we chose $\theta=0.5$. Replacing the partial derivatives by first order finite differences leads to a

tridiagonal linear equation system for each time step, which is solved by Gauß–Seidel method. The discretization is only made for $j = 0, \ldots, \max\{1 \leqslant j \leqslant N: v_j^n \geqslant \phi_c\}$.

2. The linear convective equation is solved by a second order upwind method:

$$v_j^{n+1} = v_j^n - \lambda q(t_n)(-3v_j^n + 4v_{j+1}^n - v_{j+2}^n)/2, \quad j = -2, \ldots, N.$$

3. For the hyperbolic equation, we use a modification of the Lax–Friedrichs method, the non-oscillatory central difference method (Nessvahu and Tadmor, 1990):

$$v_j^{n+1/2} = v_j^n - \lambda (f')_j^n/2,$$

$$v_j^{n+1} = \frac{1}{2}[v_{j-1}^n + v_{j+1}^n] + \frac{1}{4}[(v')_{j-1}^n - (v')_{j+1}^n] - \frac{\lambda}{2}[f_{bk}(v_{j+1}^{n+1/2}) - f_{bk}(v_{j-1}^{n+1/2})].$$

The numerical derivatives are calculated by a minmod limiter:

$$\mathrm{MM}(x, y, z) = \begin{cases} \operatorname{sgn} x \min\{|x|, |y|, |z|\} & \text{if } \operatorname{sgn} x = \operatorname{sgn} y = \operatorname{sgn} z \\ 0 & \text{otherwise,} \end{cases}$$

$$(v')_j^n = \mathrm{MM}(\kappa(v_{j+1}^n - v_j^n), \quad (v_{j+1}^n - v_{j-1}^n)/2, \quad \kappa(v_j^n - v_{j-1}^n)),$$

$$(f')_j^n = f'_{bk}(v_j^n)(v')_j^n, \quad \kappa \in [1, 4).$$

This method is second order accurate for smooth solutions of hyperbolic conservation laws and has a total variation diminishing (TVD) property for Cauchy (i.e. initial-value) problems if $\lambda \max_u |f'_{bk}(u)| \leq (\sqrt{1 + 2\kappa - \kappa^2} - 1)/\kappa$.

The boundary condition at $x = 0$ is obtained by putting $f_{bk} = 0$ wherever f_{bk} is evaluated for $x \leqslant 0$. The auxiliary solution values v_{-1}^n and v_{-2}^n are calculated in the convective step. For batch settling, we put $v_j^{n+1} = v_0^{n+1}$ for $j = -2, -1$. For the boundary condition at $x = 1$, we note that in the examples presented in this work, we can always set $v_j^{n+1} = \phi_1$ (t_{n+1}) for $j \geqslant N$. In general, entropy boundary conditions have to be considered (Bürger and Wendland, 1998b), which take into account that condition (18) is not always satisfied in the pointwise sense. This is the case if the sediment level $\phi = \phi_c$ rises above feeding level, that is, when the thickener overflows.

In some examples, the excess pore pressure p_e is calculated by a discrete version of (13) and (14),

$$(p_e)_N^n = 0, \quad (p_e)_{j-1}^n = (p_e)_j^n + L\Delta x \Delta \rho g v_j^n r_j^n, \quad r_j^n = 1 - \frac{a(v_j^n)}{f_{bk}(v_j^n)} \frac{v_j^n - v_{j-1}^n}{\Delta x}$$

and in one example, the local solid and liquid phase velocities v_s and v_f are calculated by

$$(v_s)_j^n = L\left[q(t_n) + \frac{f_{bk}(v_j^n) r_j^n}{v_j^n}\right], \quad (v_f)_j^n = L\left[q(t_n) - \frac{f_{bk}(v_j^n) r_j^n}{1 - v_j^n}\right].$$

In all calculations, we used the parameters $\Delta x = 1/400$ and $\kappa = 1.3$.

4.2. Experimental data

We consider a Kynch batch flux density function of the type introduced by Richardson and Zaki (1954) and an effective solid stress function with parameters obtained by experimental measurements (Becker, 1982):

$$\hat{f}_{\mathrm{bk}}(\phi) = -6.05 \times 10^{-4}\phi(1-\phi)^{12.59}\,\mathrm{m\ s^{-1}},$$
$$\sigma_{\mathrm{e}}(\phi) = \begin{cases} 0 & \text{for } \phi < \phi_{\mathrm{c}} = 0.23 \\ 5.35\exp(17.9\phi)\ \mathrm{Pa} & \text{for } \phi \geq \phi_{\mathrm{c}}. \end{cases} \tag{19}$$

However, the approach (19) leads to a discontinuous diffusion coefficient for which the mathematical analysis is not valid. So we introduce a function ψ which smoothes out the jump that the factor $\sigma_{\mathrm{e}}'(u)/u$, occurring in the definition (12) of $a(u)$, contains. We assume that the smoothing function is valid on a transition interval $[\phi_{\mathrm{c}},\phi_{\mathrm{c}}+\delta]$, and define ψ to be the cubic polynomial satisfying $\psi(\phi_{\mathrm{c}}) = 0$, $\psi'(\phi_{\mathrm{c}}) = 0$, $\psi(\phi_{\mathrm{c}}+\delta) = \sigma_{\mathrm{e}}(\phi_{\mathrm{c}}+\delta)/(\phi_{\mathrm{c}}+\delta)$ and

$$\psi'(\phi_{\mathrm{c}}+\delta) = \{\sigma_{\mathrm{e}}'(\phi_{\mathrm{c}}+\delta)[\phi_{\mathrm{c}}+\delta] - \sigma_{\mathrm{e}}(\phi_{\mathrm{c}}+\delta)\}/(\phi_{\mathrm{c}}+\delta)^2.$$

The resulting diffusion coefficient is

$$a(u) = -\frac{f_{\mathrm{bk}}(u)}{L\Delta\rho g}\begin{cases} 0 & \text{for } u < \phi_{\mathrm{c}}, \\ \psi(u) & \text{for } \phi_{\mathrm{c}} \leq \phi_{\mathrm{c}}+\delta, \\ \sigma_{\mathrm{e}}'(u)/u & \text{for } u > \phi_{\mathrm{c}}+\delta. \end{cases} \tag{20}$$

We use the parameters $g = 9.81\ \mathrm{m\ s^{-2}}$, $\Delta\rho = 1500\ \mathrm{kg\ m^{-3}}$ and $L = 1.742$ m, $L = 2$ m or $L = 6$ m. Fig. 2 shows the Kynch batch flux density function f_{bk} and the resulting diffusion coefficient with $\delta = 0.01$ and $L = 6$ m.

We note that the parameter λ, given in the numerical examples, refers to the transformation to feeding level height one and a time unit of 10,000 s, which is more convenient for numerical

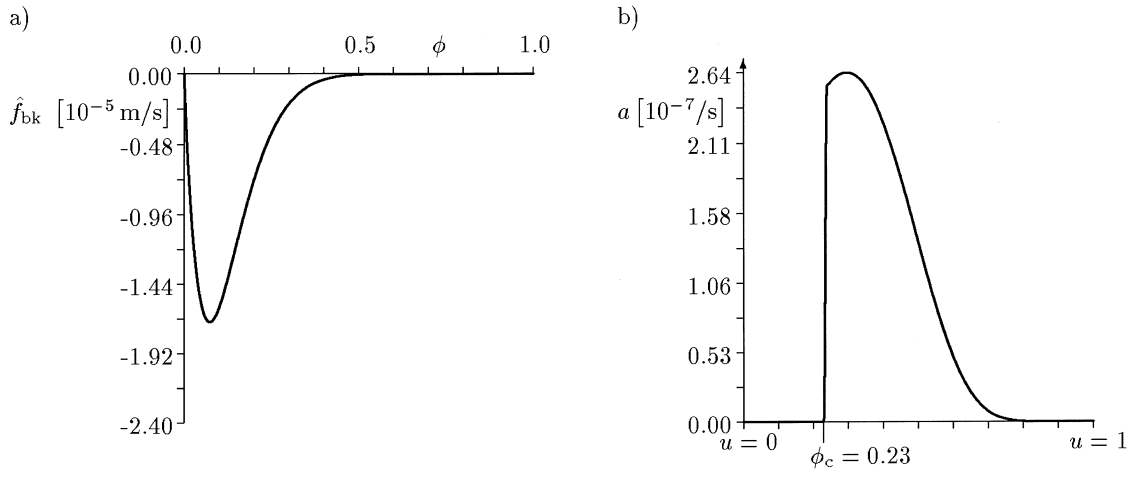

Fig. 2. (a) Kynch batch flux density function $\hat{f}_{\mathrm{bk}}$; (b) the diffusion coefficient $a(u)$ for feeding level height $L = 6$ m.

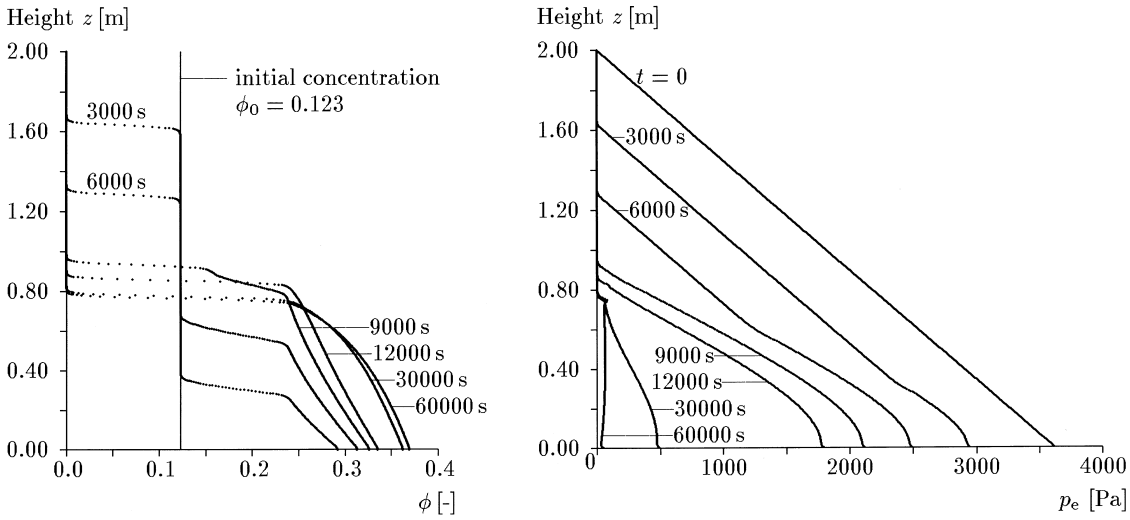

Fig. 3. Concentration and excess pore pressure profiles for batch sedimentation with compression $\lambda = 0.01$. The profiles shown correspond to the indicated times.

calculations. Thus, calculations were made for the unit interval as spatial domain, with the thickener height being considered by the parameter L in the denominator of $a(u)$.

4.3. Batch settling

4.3.1. Example 1: batch settling of a uniform suspension.

Consider a suspension of initial concentration $\phi_0 = 0.123$ in a settling column of height $L = 2$ m. Fig. 3 shows some concentration and excess pore pressure profiles, Fig. 4, the corresponding profiles of solid and fluid phase velocities and Fig. 5 the settling plot for a simulated sedimentation time of $T = 60{,}000$ s. We note that the 400 discrete solution points of the concentration profiles have been interpolated linearly, and that the concentration line $\phi = 0.11$ produced by the numerical solutions in Figs. 5 and 8 of example 3 appears where the discontinuity between zero and ϕ_0 of the exact solution is located.

4.3.2. Example 2: comparison with experimental measurements.

To compare the results of the phenomenological theory and of the numerical method with experiments, we use the result of Been and Sills (1981). They studied the sedimentation of a suspension of soft soil in a settling column of height $L = 1.742$ m with an initial concentration of $\phi_0 = 0.05264$. The experimental data, which were presented graphically by Been and Sills, lead to the following constitutive equations:

$$\hat{f}_{\mathrm{bk}}(\phi) = \begin{cases} -1.39 \times 10^{-4}\phi(1-\phi)^{28.59} \text{ m s}^{-1} & \text{for } \phi \leq = \frac{1}{12}, \\ -8.0 \times 10^{-9}\phi^2 \exp(0.7675(1-\phi)/\phi) \text{ m s}^{-1} & \text{for } \phi > \phi_c \end{cases}$$

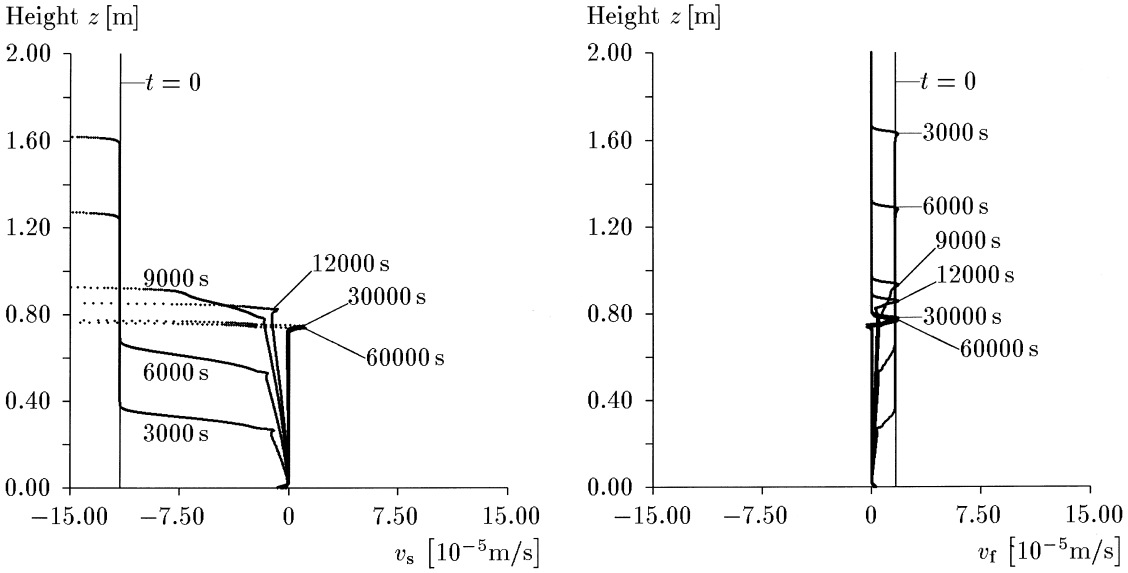

Fig. 4. Solid and fluid phase velocity profiles for batch sedimentation with compression; the profiles shown correspond to the indicated times.

and

$$\sigma_e = \begin{cases} 0 & \text{for } \phi \le \phi_c \\ 4.0\exp(21.265\phi)\ \text{Pa} & \text{for } \phi > \phi_c. \end{cases}$$

The result is shown in Fig. 6 where Been and Sills' settling plot is compared with our predictions. Note that the suspension or sediment mass densities measured by Been and Sills

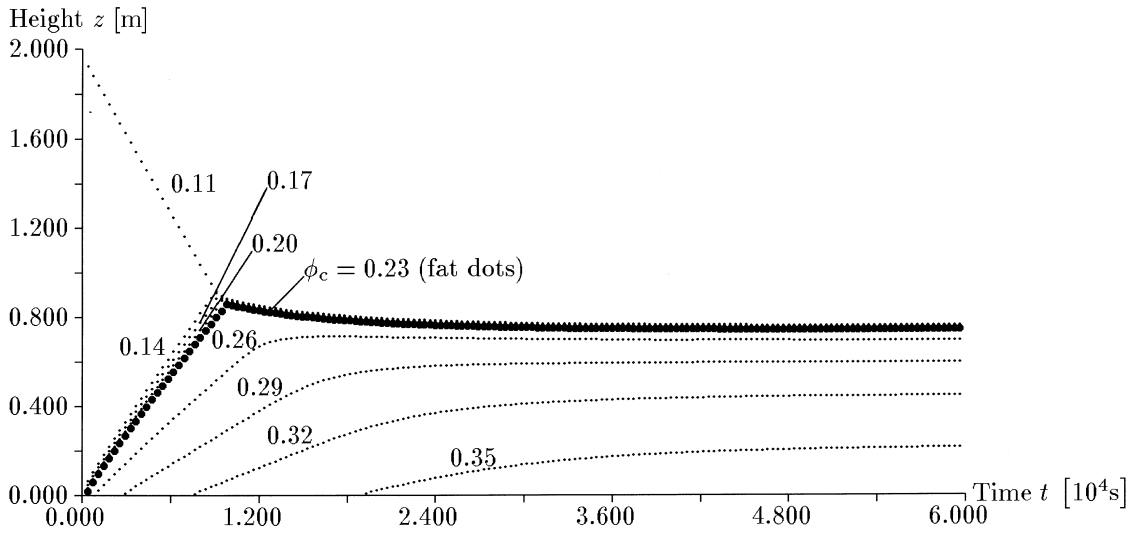

Fig. 5. Settling plot for batch settling showing sedimentation with compression using $\lambda = 0.01$ and $T = 60{,}000$ s. The dotted lines correspond to the annotated concentration values.

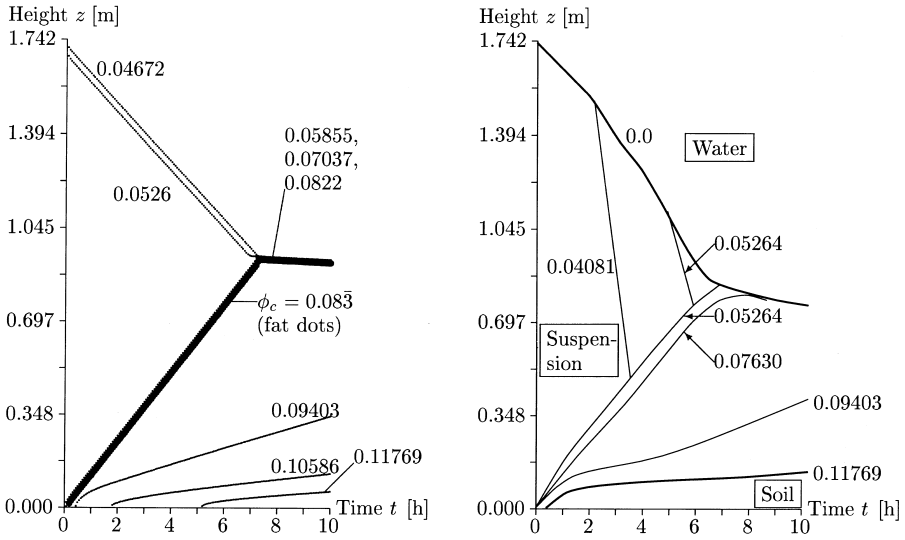

Fig. 6. Comparison of the simulation with the experimental settling plot of Been and Sills (1981).

have been transformed into volumetric solid concentrations. The corresponding excess pore pressure profiles are given in Fig. 7.

4.3.3. Example 3: repeated batch sedimentation.

An interesting modification of the previous example is obtained if we suppose that after a certain time interval the pure liquid above the (nearly) compressed sediment is replaced again by suspension of the initial homogeneous concentration ϕ_0. We consider the same data as used

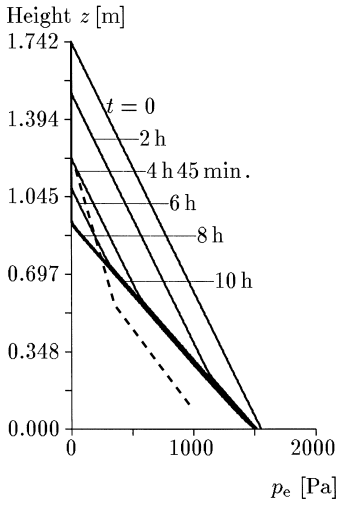

Fig. 7. Excess pore pressure profiles at indicated times. The dashed line corresponds to the excess pore pressure profile at $t = 4$ h 45 min given by Been and Sills (1981).

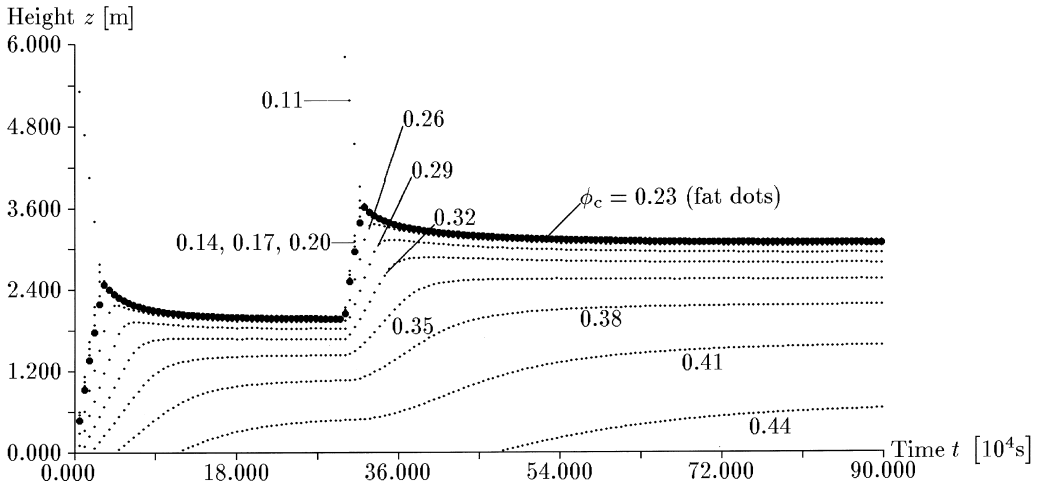

Fig. 8. Settling plot for repeated batch sedimentation using $\lambda = 0.2$ and $T = 900{,}000$ s. The dotted lines correspond to the annotated concentration values.

in example 1, but for $t = 300{,}000$ s, all concentration values less than ϕ_c are replaced by $\phi_0 = 0.123$. Fig. 8 shows the corresponding numerical simulation.

4.3.4. Example 4: expansion of overcompressed sediment.

In our last example (Fig. 9) for batch thickening, we consider a settling column of height 2 m (i.e. batch sedimentation: $q \equiv 0$ and $\phi_1 \equiv 0$) which at $t = 0$ is assumed to contain, in its lower 20%, an overcompressed sediment of concentration 0.6:

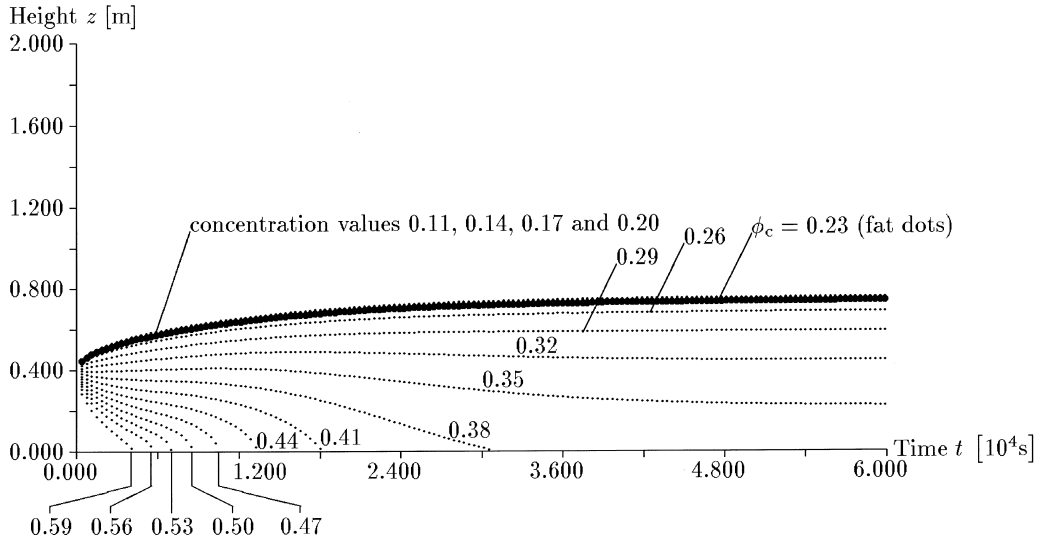

Fig. 9. Concentration lines for expansion of overcompressed sediment using $\lambda = 0.02$ and $T = 60{,}000$ s. The dotted lines correspond to the annotated concentration values.

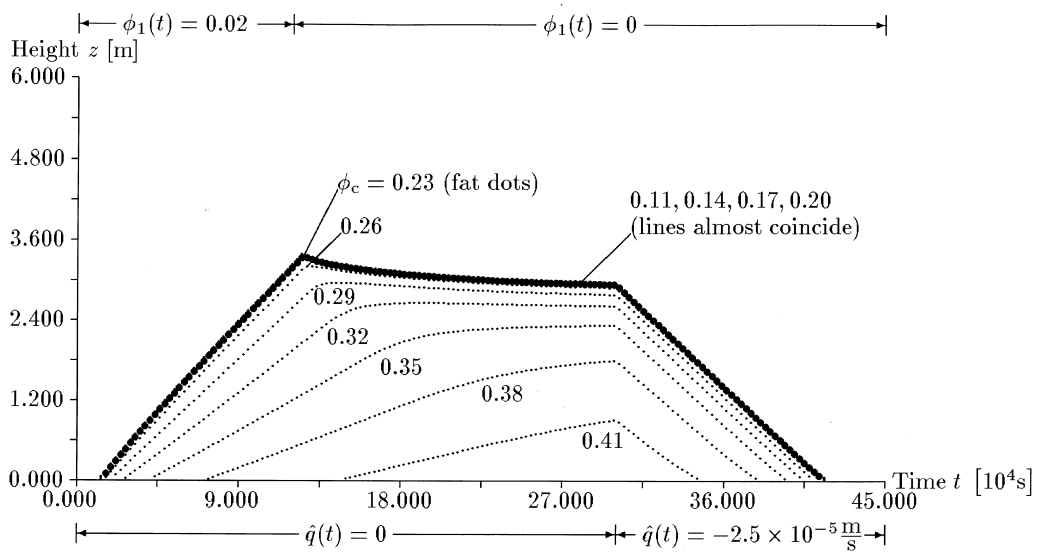

Fig. 10. Continuous thickening: numerical solution for filling up and emptying of a thickener using $\lambda = 0.125$ and $T = 45{,}000$ s. The dotted lines correspond to the annotated concentration values.

$$\phi_0(z) = \begin{cases} 0.6 & \text{for} \quad 0 \le z \le 0.4 \text{ m}, \\ 0 & \text{for} \quad 0.4 \text{ m} < z \le 2 \text{ m}. \end{cases}$$

We observe that at $t = t_0$ the sediment immediately starts to expand and tends to an equilibrium state with the sediment–liquid interface at a height of about 0.72 m. This expansion after coming in contact with water is due to the description of the solid component as an elastic fluid.

4.4. Continuous thickening

4.4.1. Example 5: the filling and emptying of a thickener.

Fig. 10 shows the settling plot for this example. We start with a thickener full of water, $\phi_0 \equiv 0$, with a feeding level height of $L = 6$ m. Its discharge is kept closed for $0 \leqslant t \leqslant 300{,}000$ s and then opened to obtain:

$$\hat{q}(t) = \begin{cases} 0 & \text{for } 0 \le t \le 300{,}000 \text{ s}, \\ -2.5 \times 10^{-5} \text{ m s}^{-1} & \text{for } 300{,}000 \text{ s} < t \le T = 450{,}000 \text{ s}. \end{cases}$$

For $0 < t \leqslant 120{,}000$ s, the thickener is fed with a feeding flux density of

$$\hat{f}_F = -9.3826 \times 10^{-6} \text{ m s}^{-1}$$

and at $t = 120{,}000$ s the feeding is discontinued, $\hat{f}_F = 0$. Since $\hat{f}_F = \hat{f}_{bk}(0.02)$, this is equivalent to prescribing $\phi_1 = 0.02$, i.e. we choose

$$\phi_1(t) = \begin{cases} 0.02 & \text{for } 0 < t \le 120{,}000 \text{ s}, \\ 0 & \text{for } 120{,}000 \text{ s} < t \le T = 450{,}000 \text{ s}. \end{cases}$$

We observe that the sediment rises at almost constant speed. At $t = 120{,}000$ s, a discontinuity between the concentration values zero and 0.02 starts to propagate from $z = H$ into the thickener at a speed of

$$s = \hat{f}_{\mathrm{bk}}(0.02)/0.02 = -4.6913 \times 10^{-4} \text{ m s}^{-1}$$

and arrives at the sediment level at an approximate height of 3.30 m at

$$t = 120{,}000 \text{ s} + 2.70 \text{ m}/s \approx 125755 \text{ s}.$$

Since the thickener remains closed, the sediment compresses further by its own weight, until the thickener is opened at $t = 300{,}000$ s. It has emptied entirely by $t \approx 435{,}000$ s.

4.4.2. Example 6: the transition between steady states.

Next, we consider steady states and transitions between them. A steady state is the mode in which a continuous thickener is expected to operate normally in industrial applications. It is fed with a suspension of constant concentration such that the feeding solid volume flux density $\hat{f}_{\mathrm{F}} = \hat{f}(\phi_1, t) = \hat{q}\phi_1 + \hat{f}_{\mathrm{bk}}(\phi_1)$ and its discharge solid volume flux density $\hat{f}_{\mathrm{D}} = \hat{q}\phi(0, t)$ are equal, $\hat{f}_{\mathrm{F}} = \hat{f}_{\mathrm{D}}$. The conditions for the existence of a steady state can be obtained by considering time-independent solutions of Eq. (17), i.e. of the ordinary differential equation

$$\hat{q}\phi' + \hat{f}'_{\mathrm{bk}}(\phi)\phi'(z) = \left(-\frac{\hat{f}_{\mathrm{bk}}(\phi)\sigma'_{\mathrm{e}}(\phi)}{\Delta\rho g\phi}\phi'(z) \right)' \Rightarrow \hat{q}\phi + \hat{f}_{\mathrm{bk}}(\phi) + \frac{\hat{f}_{\mathrm{bk}}(\phi)\sigma'_{\mathrm{e}}(\phi)}{\Delta\rho g\phi}\phi'(z) = C.$$

We assume that a desired discharge concentration ϕ_{D} is given, from which, by the boundary condition at $z = 0$, we conclude that the integration constant must equal $C = \hat{q}\phi_{\mathrm{D}}$. Thus, the concentration profile in the compression zone results in the solution of the ordinary initial value problem

$$\phi'(z) = -\frac{\Delta\rho g\phi}{\sigma'_{\mathrm{e}}(\phi)\hat{f}_{\mathrm{bk}}(\phi)}(\hat{q}\phi + \hat{f}_{\mathrm{bk}}(\phi) - \hat{q}\phi_{\mathrm{D}}), \quad z > 0 \tag{21}$$

$$\phi(0) = \phi_{\mathrm{D}}.$$

Eq. (21) is integrated up to the value $\phi(z) = \phi_{\mathrm{c}}$. For sedimentation to take place, $\phi'(z) \leqslant 0$, that is

$$\hat{q}\phi + \hat{f}_{\mathrm{bk}}(\phi) \leq \hat{q}\phi_{\mathrm{D}} \text{ for } \phi \in [\phi_{\mathrm{c}}, \phi_{\mathrm{D}}]$$

must be satisfied so that the right hand side of Eq. (21) is nonpositive (see Concha et al., 1996). If the flux density function possesses a local maximum at $\phi = \phi_{\mathrm{M}}$, then the condition $\phi_{\mathrm{c}} < \phi_{\mathrm{D}} < \phi_{\mathrm{D}_{\max}}$, where $\phi_{\mathrm{D}_{\max}}$ is obtained by $\hat{f}(\phi_{\mathrm{M}}) = \hat{q}\phi_{\mathrm{D}_{\max}}$, must be satisfied. In the case of a monotonically decreasing flux density function, $\phi_{\mathrm{D}_{\max}}$ is given by $\hat{f}(\phi_{\mathrm{c}}) = \hat{q}\phi_{\mathrm{D}_{\max}}$. The boundary value at $z = L$ is obtained by solving the equation

$$\hat{f}(\phi_1) = \hat{q}\phi_{D_{max}}, \quad \phi_1 < \phi_{\mathrm{M}}$$

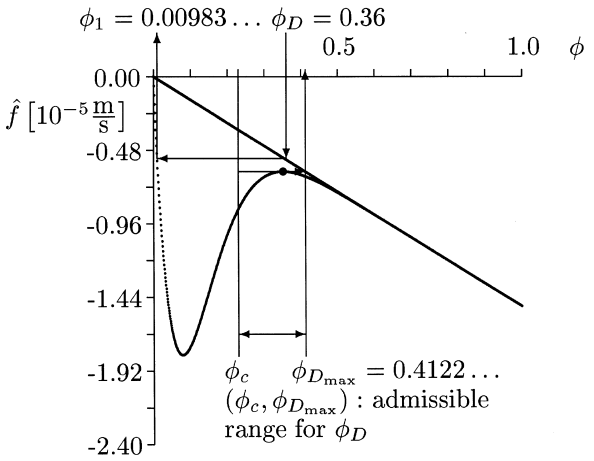

Fig. 11. The set of admissible discharge concentrations and the construction of the boundary datum ϕ_1 for $\phi_D = 0.36$ for $\hat{f}(\phi) = \hat{q}\phi + \hat{f}_{bk}(\phi)$ with $\hat{q} = -1.5 \times 10^{-5}$ m s^{-1} and $\phi_c = 0.23$.

for ϕ_1. Fig. 11 shows an example for the construction of $\phi_{D_{max}}$ and of ϕ_1 for a given value of ϕ_D.

We now consider a numerical example of transitions between (approximate) steady states. We calculated the following steady states $\phi_i(z)$, $i = 1,2,3$ in advance for a feeding level height of $L = 6$ m:

i	$\hat{q}^i$ [10^{-5} m s^{-1}]	ϕ_D^i	$\hat{f}_F^i = \hat{f}_D^i$ [10^{-5} m s^{-1}]	ϕ_1^i	Sediment height λ_i [m]
1	-1.5	0.36	-0.54	0.00983189	1.00
2	-0.5	0.42	-0.21	0.00369112	2.49
3	-3.0	0.35	-1.05	0.02139377	1.54

We choose the steady state $\phi_1(z)$ as the initial state in the continuous thickener, $\phi_0(z) = \phi_1(z)$, and choose the boundary datum $\phi_1(t) = \phi_1^1$ correspondingly. At $t = 50{,}000$ s, we change to the next steady state. Therefore at that time $\hat{q}$ is changed from $\hat{q}^1$ to $\hat{q}^2$, causing a rise of the sediment level. As the feeding flux density remains constant during this change, we have to change $\phi_1(t)$ from ϕ_1^1 to ϕ_1^{1*}, which has to be calculated from

$$\hat{f}_F^1 = \hat{q}^2\phi_1^{1*} + \hat{f}_{bk}(\phi_1^{1*}),$$

resulting, in this case, in $\phi_1^{1*} = 0.010040585$. The sediment rises at an apparently constant velocity of 0.97×10^{-5} m s^{-1} and reaches the sediment level λ_2 at $t = 205208$ s. Taking into account the propagation velocity of the discontinuity between ϕ_1^{1*} and ϕ_1^2, the change of $\phi_1(t)$ is made at $t = 198{,}350$ s. We observe that the sediment tends toward the calculated second steady state, and that the discharge concentration approximates the corresponding value

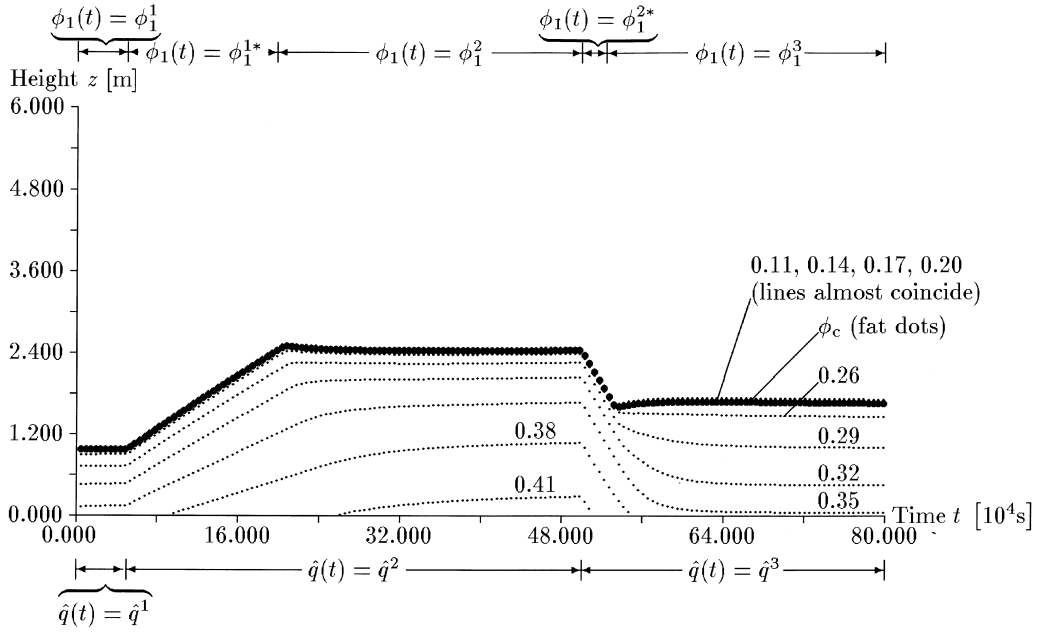

Fig. 12. Settling plot for continuous sedimentation with transition between approximate steady states using $\lambda = 0.1$ and $T = 800{,}000$ s. The dotted lines correspond to the annotated concentration values.

$\phi_D^2 = 0.42$. At $t = 500{,}000$ s, we change $\hat{q}(t)$ from $\hat{q}^2$ to $\hat{q}^3$, and by the continuity of the feeding flux, $\phi_1(t)$ from ϕ_1^2 to ϕ_1^{2*}. The value $\phi_1^{2*} = 0.003532479$ is obtained from

$$\hat{f}_F^2 = \hat{q}^3\phi_1^{2*} + \hat{f}_{bk}(\phi_1^{2*}).$$

The sediment level will have fallen to λ_2 by $t = 538{,}434$ s. The change from ϕ_1^{2*} to ϕ_1^3 has to be carried out before, such that $\phi(z, t) = \phi_1^3$ is valid above the sediment level for $t \geqslant 538{,}434$ s. The change from ϕ_1^{2*} to ϕ_1^3 causes a rarefaction wave propagating into the thickener. From the speed at which the value $\phi = \phi_1^3$ propagates, we obtain that the boundary value $\phi_1(t)$ has to be changed at $t = 524{,}697$ s. The desired third steady state $\phi_3(z)$ is approximated well by the concentration profile at $t = T = 800{,}000$ s, when the simulation ends. Fig. 12 shows the settling plot for this simulation.

5. Discussion

The phenomenological theory of sedimentation with compression outlined in the first part of this paper had been proposed before by one of the authors (e.g. in Concha et al., 1996). It has been analyzed and used so far for the simulation of settling behaviour only under additional restrictive assumptions which permit an explicit construction of the exact solution. In particular, the hyperbolic equations and their boundary problems for piecewise constant data for batch and continuous sedimentation corresponding to Kynch theory have been studied thoroughly, a formal mathematical framework therefore has been established, and

sedimentation processes have been classified (Bustos et al., 1990a,b; Bustos and Concha, 1996; Concha and Bürger, 1998). Moreover, steady states for sedimentation with compression have been constructed explicitly (Concha et al., 1996). This paper shows that these results can be extended to continuous sedimentation with compression. The formal existence and uniqueness results (Bürger and Wendland, 1998a) are necessary to be able to calculate a numerical solution at all, and the jump and entropy conditions (Bürger and Wendland, 1998b) indicate which properties the exact solution, and eventually the numerical algorithm, should possess. Our numerical algorithm is constructed in a straightforward manner, however it still remains to prove its convergence formally. Nevertheless, the presented numerical examples indicate that it works well for practical purposes. The batch sedimentation example 2 agrees well with Been and Sills' experimental measurements. Example 3 refers to some industrial applications. Furthermore, the numerical solutions throw up new challenging tasks for the analysis of the mathematical model, e.g. it should be desirable that the convergence to steady state takes place in a finite period of time. Example 5 shows that the boundary conditions sensibly model the operation of a continuous thickener, and that the filling up from a pure liquid state and the emptying of the thickener can be modelled. Example 6 corresponds to the most interesting industrial application, namely the prediction of the behaviour of the sediment between steady states. Here we observe a stabilization effect, i.e. if the feeding and discharge conditions belong to a steady state, the sediment "tends" to the steady state (in a sense yet to be precised) in time, even from a disturbed initial concentration. Moreover, it should be possible to show formally that the observed linear growth of the sediment level during transition from a steady state is a property inherent to the mathematical model, which would allow the construction of a control model for continuous sedimentation similar to the model in Bustos et al. (1990b) for the hyperbolic case. All these examples show that our model works reasonably for most applications, but the expansion of sediment simulated in example 4 is not observed in nature. Example 4 alerts us to the fact that modelling the solid component as an ideal fluid has its limitations and that a different model should be sought.

Acknowledgements

This work was supported by the German Research Foundation (DFG) Collaborative Research Programme (Sonderforschungsbereich) 404 at the University of Stuttgart, by Fondecyt project 89/352, by the University of Concepción Research Council through project DI 92.95.044-1 and by Fundación Andes, project C-13131 at the University of Concepción.

References

Becker, R. 1982. Continuous thickening, design and simulation of thickeners. Habilitación professional. University of Concepción.

Been, K., Sills, G.C., 1981. Self-weight consolidation of soft soils: an experimental and theoretical study. Géotechnique 31, 519–535.

Bürger, R., 1996. Ein Anfangs-Randwertproblem einer quasilinearen parabolischen entarteten Gleichung in der Theorie der Sedimentation mit Kompression. Doctoral thesis, University of Stuttgart.

Bürger, R., Wendland, W.L., 1998a. Existence, uniqueness and stability of generalized solutions of an initial-boundary value problem for a degenerating quasilinear parabolic equation. J. Math. Anal. Appl. 218, 207–239.

Bürger, R., Wendland, W.L. 1998b. Entropy boundary and jump conditions in the theory of sedimentation with compression. Math. Meth. Appl. Sci. 21, 865–882.

Bustos, M.C., Concha, F., 1996. Kynch theory of sedimentation. In: E. Tory (Ed.). Sedimentation of Small Particles in a Viscous Fluid. Computational Mechanics Publications, Southampton.

Bustos, M.C., Concha, F., Wendland, W.L., 1990a. Global weak solutions to the problem of continuous sedimentation of an ideal suspension. Math. Meth. Appl. Sci. 13, 1–22.

Bustos, M.C., Paiva, F., Wendland, W.L., 1990b. Control of continuous sedimentation of ideal suspensions as an initial and boundary value problem. Math. Meth. Appl. Sci. 12, 533–548.

Coe, H.S., Clevenger, G.H., 1916. Methods for determining the capacity of slimesettling tanks. Trans. AIME 55, 356–385.

Concha, F., Barrientos, A., 1993. A critical review of thickener design methods. KONA no. 11, 79–104.

Concha, F., Bürger, R. 1998. Wave propagation phenomena in the theory of sedimentation. In: Toro, E. F., Clarke, J. F. (Eds) Numerical Methods for Wave Propagation Problems. Kluwer, Dordrecht, in print.

Concha, F., Bustos, M.C., Barrientos, A. 1996. Phenomenological theory of sedimentation. In: Tory, E. (Ed) Sedimentation of Small Particles in a Viscous Fluid. Computational Mechanics Publications, Southampton, pp. 51–96.

Kynch, G.J., 1952. A theory of sedimentation. Trans. Farad. Soc. 48, 166–176.

Landman, K.A., White, L.R., 1994. Solid/liquid separation of flocculated suspensions. Adv. Colloid Interface Sci. 51, 175–246.

Mishler, R.T., 1912. Settling slimes at the Tigre Mill. Eng. Mining J. 94 (14), 643–646.

Nessyahu, H., Tadmor, E., 1990. Non-oscillatory central differencing for hyperbolic conservation laws. J. Comp. Phys. 87, 408–463.

Richardson, J.F., Zaki, W.N., 1954. Sedimentation and fluidization I. Trans. Inst. Chem. Eng. (London) 32, 35–53.

Tory, E. 1996. Sedimentation of Small Particles in a Viscous Fluid. Computational Mechanics Publications, Southampton.

Whitaker, S., 1986. Flow in porous media I: a theoretical derivation of Darcy's law. Transp. Porous Media 1, 3–25.